Article

Positive-Charge-Based Small Molecule Dyes for Gut Microbiota Fluorescent Imaging

Yue Liu,[¶] Zhiming Wang,[¶] Ke Li, Ruihu Song, Zhiqiang Xu, Tianhe Yu, Jing Wang, Xin Feng,* and Hao Chen*

Cite This: *ACS Omega* 2024, 9, 36371−36379

Read Online

ACCESS | Metrics & More | Article Recommendations | Supporting Information

ABSTRACT: As one of the research hotspots in recent years, gut microbiota have been proven to be closely related to host metabolism, nutrient absorption, and immune regulation. However, there are still many urgent issues in the research of gut microbiota, such as the localization and tracking of gut microbiota. In this research, two new fluorescent probes, EF and 6F, were developed by optimizing the structure of the positron salt small molecule probe F16. *In vitro* labeling experiments showed that EF and 6F can quickly label Gram-positive bacteria, *Staphylococcus aureus* and *Lactobacillus reuteri*, as well as Gram-negative bacteria, *Escherichia coli* and *Salmonella pullorum*. Meanwhile, EF and 6F have little bacterial toxicity and are used at a maximum concentration of 200 μM. Compared with EF, 6F has better hydrophilicity and stronger fluorescence characteristics in aqueous solutions, making it more suitable for imaging within gut microbiota populations. The results of *in vivo* imaging experiments indicate that EF and 6F can label and image the intestinal microbiota colonized by the mouse intestinal mucosal epithelium without causing any damage to intestinal tissue. Compared with commercially available MitoTracker dyes and fluorescein 5-isothiocyanate (FITC) dyes, EF and 6F exhibit better biocompatibility. Therefore, the compounds EF and 6F synthesized in this study are novel small molecule probes suitable for imaging gut microbiota, providing a better probe selection for exploring complex gut microbiota.
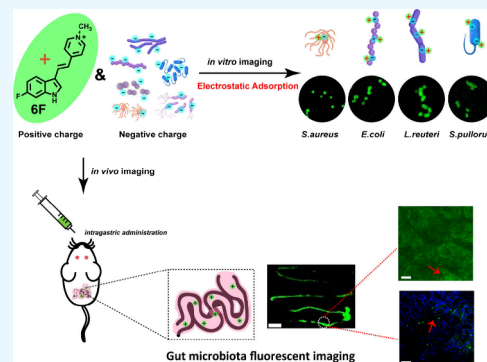
1. INTRODUCTION

The human gut, in which about ten trillion symbionts live, is a complex microecological system collectively known as microbiota.[1] It has a vital role in the host's metabolism, immunity, and inflammation during the host's whole life.[2] Usually, the individual's microbiota is thought to be unique. Therefore, people believe that dietary habits and mental and physical health could be revealed by classifying and identifying the bacteria.[3,4] Currently, gastrointestinal microbiome identification highly relies on high-throughput DNA sequencing of the fecal microbiome.[5] It is controversial whether the fecal microbiome can represent the whole composition of the colonized bacteria in the gut.[6,7] Simultaneously, many problems still need to be solved in the research of the gut microbiota, such as the localization and tracking of microbiota, dynamic monitoring of microbiota, and interactions between gut microbiota. The existing research methods cannot meet the needs of growing gut microbiota research. The intestinal flora is composed in a particular proportion to form a stable ecosystem where bacteria cooperate and restrain each other. Many foreign bacteria cannot colonize in the intestinal tract and are excreted with feces. The composition of bacteria in feces exceeds that of the colonized gut microbiota. Therefore, new tools that can detect the microbiota and where it exists in

the digestive tract are urgently needed.[8] Gut microbe imaging could be a suitable method to resolve this problem.[9]

Various recent attempts have been made to develop convenient bacteria imaging methodologies. At first, the bacteria were engineered by transferring fluorescent protein genes into bacterial genes.[10,11] However, most gut microbiota are hard to isolate and culture in artificial conditions, making gene transfer difficult.[12] Then, the bacteria were labeled by specifically binding to bacterial nucleic acid sequences, such as fluorescence in situ hybridization (FISH).[13] It is regrettable that FISH can only mark the dead bacteria. Then, researchers attempted to find a way to label the bacteria *in vivo* to reveal the relationship between the bacteria's division and the host's health. Since some antibiotics can specifically bind to the bacterial outer membrane, bacterial fluorescent probes were prepared by combining antibiotics with fluorescent dyes to selectively label bacteria in complicated samples.[14−16] The biggest concern for these probes is toxicity. Usually, even low
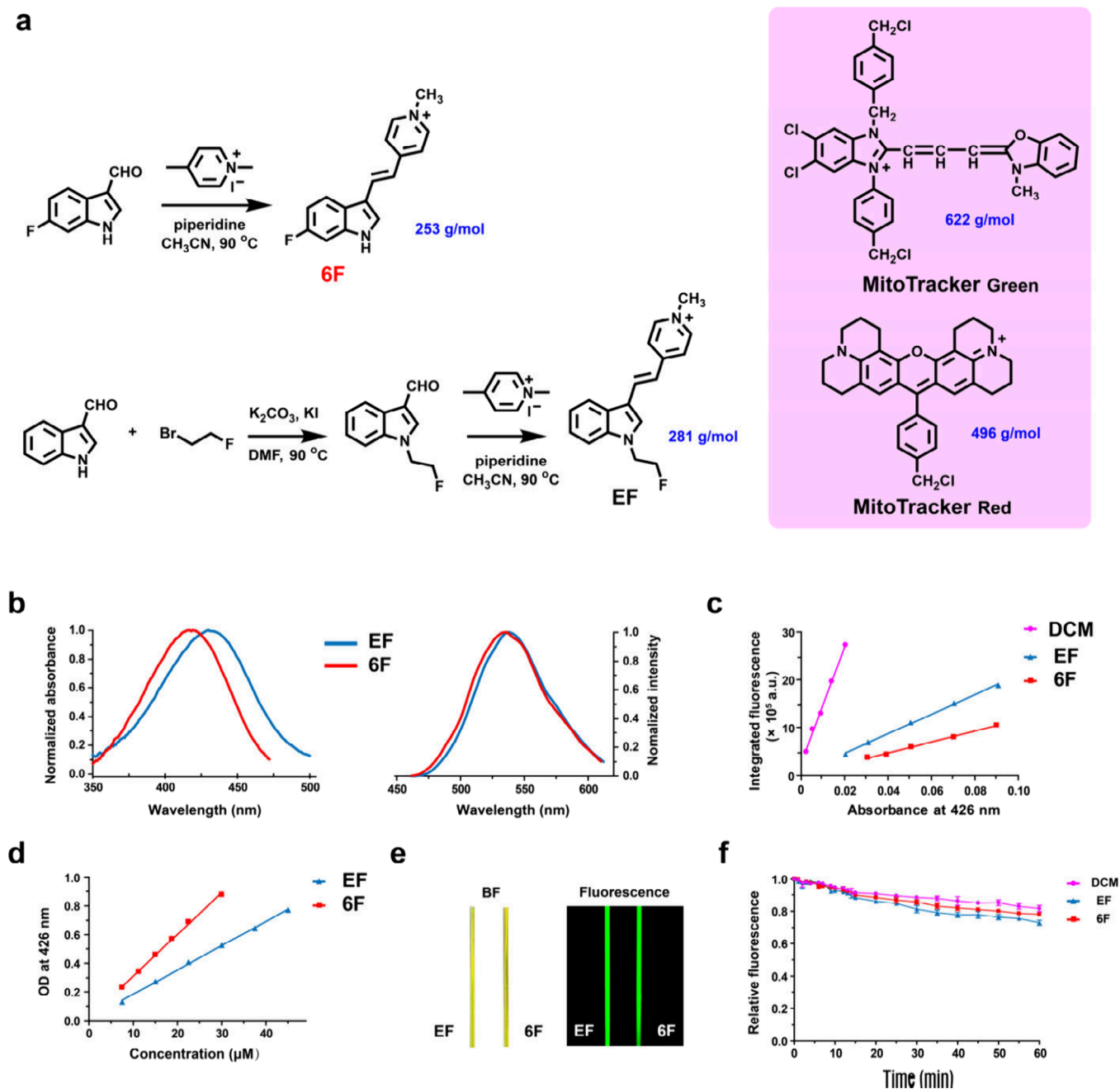
Figure 1. Synthesis and characterization of EF and 6F. (a) Structure and synthetic route of EF and 6F. The chemical structures of EF and 6F are more simple than those of the commercially available MitoTracker Red and MitoTracker Green. (b) Normalized absorption (left) and emission (right) spectrum of EF and 6F, which were measured in water. (c) Quantum yields of EF and 6F (measured in acetonitrile, DCM QY = 43% as the standard sample). (d) Molar absorption coefficient (ε) of EF and 6F (measured in water). (e) Brightfield (BF) and fluorescent images of 20 μM EF (left) and 6F (right) in a capillary pipet. (f) Photostability of EF, 6F, and DCM at a concentration of 20 μM in water.

concentrations of antibiotic-based imaging probes would damage bacteria vitality, resulting in drug resistance and host-microbiota disorder.[17,18] Then, some studies tried to label bacteria using metabolic labeling strategies. During proliferation or getting energy, the bacteria bring these probes into the body, thereby realizing bacterial labeling. It has been used to track gut microbiota colonization and spatial distribution.[19] But this strategy would fail when the bacterial metabolic pathways changed, which is likely to happen in gut microbiota.

As we know, nearly all bacterial membranes have a negative surface charge.[20] Based on this, the toxic metal cations were used as a bacteria sterilant. Some studies have used contrast

reagent labeled metal cations for bacterial imaging, which faces safety concerns similar to those for antibiotic-based probes.[21] Other cation probes, like cationic peptides, could easily penetrate mammalian cells, resulting in high background noise.[22,23] The positively charged dye MitoTracker Red has been tried using *in vitro* bacteria fluorescent imaging.[24] However, it is too expensive to perform *in vivo* bacteria imaging due to the complex chemical structure needing multistep organic synthesis. FITC is one of the most widely used green fluorescein derivatives in biology, which can be used for protein markers, protein fluorescent tracers, labeled antibodies, and microsequencing of proteins and peptides

Table 1. Physicochemical Properties of Probes

compound	abs (nm)	em (nm)	Log $D_{7.4}{}^{a}$	ε (L/mol/cm)^{b}	QY (%)^{c}	$\varepsilon \times$ QY^{d}
EF	431	538	-0.17 ± 0.01	1.695×10^4	1 (8.8)	1.695×10^4
6F	421	536	0.21 ± 0.01	2.902×10^4	2.26 (4.4)	6.558×10^4

^{a}Log $D_{7.4}$ values were measured in the *n*-octanol and PBS phase ($n = 3$). ^{b}Molar absorption coefficient (ε) of EF and 6F was measured in water. ^{c}QYs of EF and 6F were measured in water and compared with DCM measurement (QY:43%). The QYs of EF and 6F in methanol were in the brackets. $^{d}\varepsilon$ and QYs multiplying results of EF and 6F in water.

(HPLC).[25] However, more research needs to be done on its *in vitro* labeling of bacteria.[26]

Herein, we report two small-molecule fluorescence dyes, EF and 6F, for microbiota-targeted imaging based on charge interaction. They can quickly label Gram-positive and Gram-negative bacteria under culture conditions with negligible toxicity. They are also stable in the acidic stomach and alkaline intestine. After intragastric administration, EF and 6F can label the gut microbiota in the distal ileum and the large intestine. Compared with EF, 6F can stay longer in the intestine with a better molar absorption coefficient, which is more suitable for future microbiota imaging. Our work provides a new probe option for exploring complex gut microbiota and provides a new bacteria labeling dye design strategy.

2. RESULTS AND DISCUSSION

### 2.1. Design, Synthesis, and Characterization of EF and 6F.
EF and 6F are the derivatives of F16 ((*E*)-4-(1*H*-indol-3-ylvinyl)-*N*-methylpyridinium iodide), which is a famous delocalized lipophilic cation for cell mitochondria imaging.[27] Driven by the mitochondrial membrane potential, they can enter the mitochondrial matrix for enrichment and imaging. In the endosymbiotic hypothesis, mitochondria were regarded as evolving from cells' symbiotic bacteria. So, we believe it may be able to stain the bacteria. Meanwhile, our previous study found that indole nitrogen alkyl substitution dramatically decreased the toxicity of F16s, demonstrating the possible good biocompatibility of some F16s. Therefore, it is highly significant to continuously improve and modify the structure of F16s to enhance their fluorescence properties and reduce their toxicity. EF was substituted on the indole nitrogen part to prove whether it was suitable for bacteria, but 6F was not. Compared to commercial dyes, MitoTracker Red CMXRos and MitoTracker Green, EF and 6F show negligible toxicity with simple chemical structures and low cost, which can be obtained from no more than two steps of organic synthesis with simple starting materials (indole-3-carbaldehyde derivatives and 1,4-dimethylpyridin-1-ium) (Figure 1a). Leaving out the negatively charged iodide or chloride part, the molecular weights of the positively charged parts of EF and 6F were 281 and 253 Da, respectively, which are much lower than those of MitoTracker Red CMXRos (496 Da) and MitoTracker Green (622 Da). Therefore, while both MitoTracker Red CMXRos and MitoTracker Green can label bacteria, EF and 6F offer more significant advantages over them. However, their undeniable effectiveness in labeling bacteria, coupled with their mitochondrial association, means that they serve as good references for EF and 6F in assessing their labeling performance.

The optical properties of EF and 6F were studied for gut microbiota imaging. They had similar optical properties, although modification of the indole ring usually significantly influences the optical properties of F16s. The absorption wavelength ranges from 350 to 500 nm, and the fluorescence emission wavelength falls between 460 and 630 nm (Figure 1b). The absorption peaks of EF and 6F were 431 and 421 nm, respectively. And the fluorescence emission peaks of EF and 6F were 538 and 536 nm (Figure 1b). The quantum yields (QYs) of EF and 6F were measured in methanol and water using 2-(2-(4-(dimethylamino)styryl)- 6-methyl-4*H*-pyran-4-ylidene) malononitrile (DCM) (QY: 43%) as reference (Figure 1c, Table 1). EF showed a higher quantum yield (8.8%) in methanol, but 6F showed a higher quantum yield (2.26%) in water. Then, the molar absorption coefficient (ε) of EF and 6F was measured in water. 6F stands out as having a higher absorbency (Figure 1d). Notably, after comparing the results of multiplying the ε and QYs in water ($\varepsilon \times$ QY), 6F shows better fluorescence properties (6.558×10^4 vs 1.695×10^4 for EF). In addition to this, both of them demonstrate good photostability (Figures 1f, Figure S1).

2.2. *In Vitro* Imaging of Bacteria Labeled with EF and 6F.
To ascertain the optimal concentration for labeling bacteria, we conducted tests on the bacterial toxicity of EF and 6F using Mito Tracker Red and Mito Tracker Green as controls. At 5 μM, the bacterial viability of Mito Tracker Red and Mito Tracker Green was nearly 50%, but that of EF and 6F was more than 90%. The toxicity of MitoTracker Red CMXRos and MitoTracker Green was much higher than that of EF and 6F (Figure 2). Unlike in mammalian cells, the indole nitrogen alkyl-substituted EF did not show better compatibility than 6F in bacteria labeling.[28,29] Common bacteria were selected for staining, including Gram-positive bacteria (*Staphylococcus aureus* and *Lactobacillus Roy*) and Gram-negative
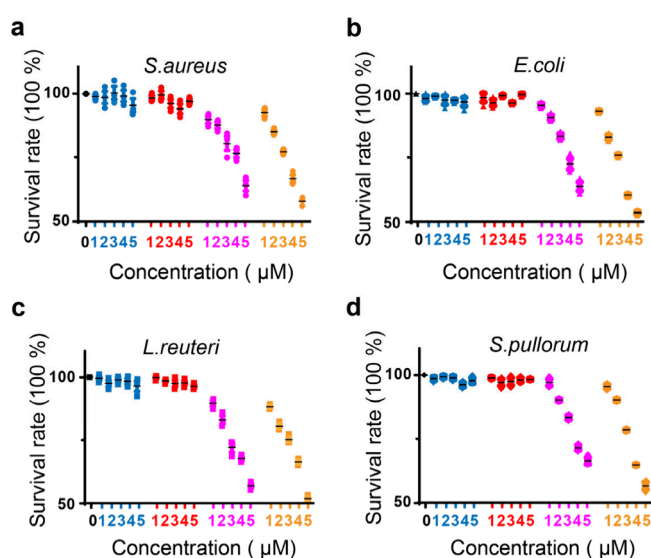
Figure 2. Toxicity of EF (blue), 6F (red), MitoTracker Red (purple), and MitoTracker Green (yellow) at different concentrations (0, 1, 2, 3, 5 μM) in (a) *S. aureus*; (b) *E. coli*; (c) *L. reuteri*; (d) *S. pullorum*. The control group is shown in black.
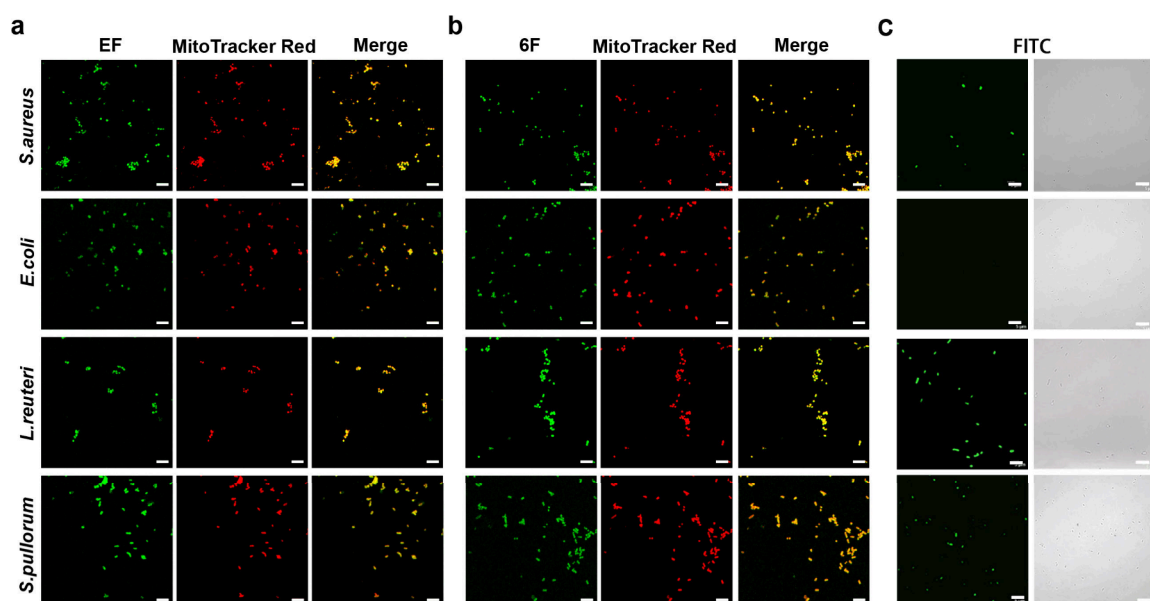
Figure 3. Fluorescent imaging of EF (a) and 6F (b) labeled bacteria. Mito Tracker Red is used as a reference. (c) FITC as another reference. Scale bars: 5 μm.

bacteria (*Escherichia coli*, *Salmonella pullorum*, and *Klebsiella pneumoniae*). The plate colony count method determined the toxicity of EF and 6F to the strains. Bacteria cocultured with EF and 6F (100, 200, 300, 500 μM). After 6 h (within 8 h), count the colony-forming unit (CFU) to calculate the bacterial viability. At 200 μM, the survival rate of bacteria exceeds 50%, but *Staphylococcus aureus* is more sensitive to probes that may be related to the outer wall structure of cells (Figure S2).

The bacterial labeling properties were tested. The labeling step occurred under normal bacterial culture conditions. First, the five strains were incubated with 200 μM EF and 6F for 20 min. After being washed three times, the bacteria were put on the glass slides and visualized by confocal fluorescence microscopy. The commercial dye MitoTracker Red CMXRos was chosen as the costaining reference, and FITC was another reference. As expected, EF and 6F labeled Gram-positive and Gram-negative bacteria, except *K. pneumoniae* (Figure 3a and b, Figure S3). FITC could only label *S. aureus*, *L. reuteri*, and *S. pullorum* (Figure 3c). It may be related to the various capsules of *K. pneumoniae*, resulting from resistance to the environment.[30] Additionally, we observed that EF and 6F exhibit distinct labeling effects on Gram-positive and Gram-negative bacteria. Overall, the labeling efficiency of Gram-positive bacteria surpasses that of Gram-negative bacteria. This disparity is attributed to the distinct composition of the cell walls in Gram-positive and Gram-negative bacteria. Gram-negative bacteria possess an outer membrane, which affects the interaction between the bacteria and the probes. Moreover, fresh bacteria were labeled more easily than aging ones (Figure S4). The logarithmic phase represents the period of optimal bacterial activity and vigorous metabolism. Selecting bacteria within this growth phase for labeling proves to be more effective than using those in stationary and death phases. Therefore, although EF and 6F primarily target bacteria via electrostatic interactions, their labeling efficacy is influenced by factors such as the structural characteristics of the bacteria and their growth stage. Interestingly, after bacteria were labeled with EF and 6F, their emission spectra exhibited minimal change. This suggests that the fluorescence properties of the

probe remain stable and are not degraded by the bacteria (Figure.S5). Then, we determined the optimal conditions for labeling bacteria through experimental validation, aiming to facilitate subsequent *in vivo* labeling procedures. Further research is warranted to investigate the targeting capabilities of probes for bacteria with varying characteristics. However, at this stage, EF and 6F suffice for our localizing and imaging needs of gut microbiota. In general, EF and 6F could effectively label Gram-positive and Gram-negative species in bacterial cultures without apparent toxicity. Then, we verified the labeling efficiency of EF and 6F *in vivo*, staining the intestine's gut microbiota.

2.3. *In Vivo* Imaging of Gut Microbiota with EF and 6F. As is known, the mammalian digestive system consists of the digestive tract and glands. Therefore, EF and 6F's stability in different artificial gastrointestinal fluids was tested first (Figure. S6). After 24 h of incubation, the fluorescence intensity of EF and 6F remained more than 85%, demonstrating EF and 6F's excellent stability in the digestive tract.

Then, two groups of 6-week old BALB/c mice under the same feeding conditions were treated with EF, 6F, and FITC (for a 20 g mouse, the dosage is 2 mg, 100 mg kg^{-1}) by intragastric administration (per = 3). Given that the inherent fluorescence of mouse fur influences the fluorescence detection spectrum of EF and 6F, we opted to conduct fluorescence imaging on the solated gastrointestinal tract and vital organs of the mice. After 4 h, the intestine and the other major organs were taken and imaged with the IVIS Lumina system. The fluorescence mainly existed in the distal ileum, cecum, and colon, with little or nearly no signal in the stomach and the front end of the small intestine (Figure 4c). The reason is that the colonizing bacteria are mainly distributed in the cecum and colon, which our probes could label. Then, fluorescent confocal endomicroscopy was used to image intestine bacteria to prove this. The labeled bacteria were found to be attached to the villus (Figure 4a,b). A small amount of gastrointestinal tissue was taken for compression, and fluorescent labeling on villi was observed with a confocal microscope. Further scraping
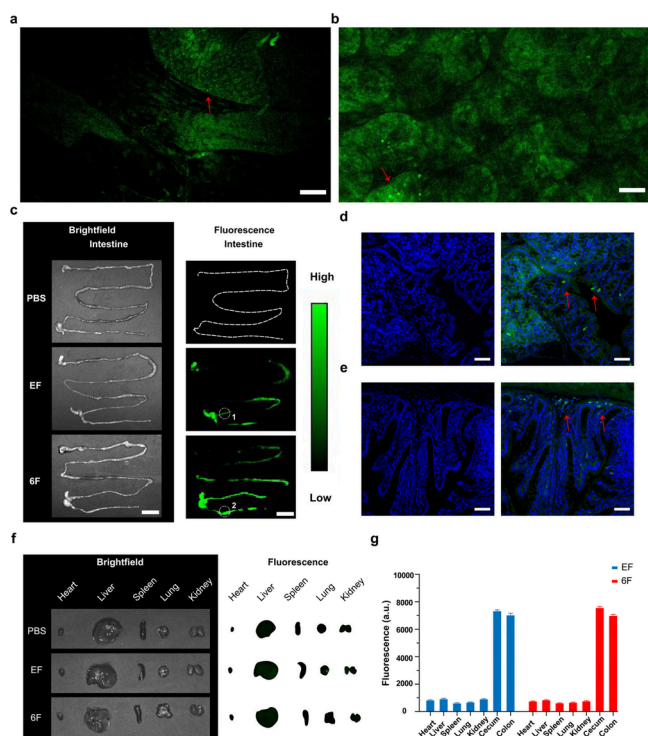
Figure 4. Fluorescent endomicroscopy images of the (a) EF and (b) 6F treated intestinal villus. (c) Ex vivo BF and fluorescent imaging of intestine in BALB/c mice after 4 h intragastric administration of PBS, EF, and 6F ($n = 3$ per group, the dosage is 100 mg kg^{-1}). The images were obtained with an exposure time of 1 s, an excitation wavelength of 465 nm, and a fluorescence wavelength of 530 nm. (d, e) Confocal microscope fluorescent imaging of ileum tissue "1" in (c) (up) and confocal microscope fluorescent imaging of colon tissue "2" in (c) (down). Red arrows mark the gut microbiota. Hoechst 33342 (blue) was used for the nuclear counterstain. Scale bars, 50 μm. (f) *Ex vivo* BF and fluorescent imaging of the major organs in BALB/c mice 4 h post intragastric administration of PBS, EF, and 6F ($n = 3$ per group). The parameter was the same with (c). (g) Fluorescent intensity quantification of different organs after intragastric administration of EF and 6F for 4 h ($n = 3$ per group).

the fluorescent spots on the villi for Gram staining can allow one to observe bacteria (Figure S7.2). These intestinal colonizing bacteria stick together to avoid being cleared by gastric acid, bile, and other gastrointestinal fluids and intestinal peristalsis. The fluorescent endomicroscopy probe could be inserted directly into the intestines of more giant animals, allowing *in vivo* imaging of gut microbiota with our probes.[31]

Then, the ileum and colon segments were imaged by confocal microscopy. After the contents were cleaned, the ileal and colonic intestines were cut into 8 μm slices. Under confocal microscopy, the bacteria were at the epithelial layer (Figure 4d and e). Interestingly, the colonizing flora was challenging to observe in past research but apparently were visible with our dyes, indicating that our probe could target these microorganisms. It seems our probe could hardly penetrate the intestinal epithelial cells, which could differentiate the bacteria from the cells and effectively minimize the interference of background fluorescence from biological tissues. Meanwhile, no apparent intestine damage was found by H&E staining compared with the mice treated with PBS (Figure S7.1, Figure S8). The fluorescence intensity quantification between the intestine and other organs is

summarized in Figure 4f and g. The other main organs had nearly no fluorescence, demonstrating that EF and 6F could not be absorbed by intragastric administration (Figure 4f), which is crucial for gut microbiota imaging. Furthermore, we counted the fluorescence intensity of the intestine and organs in the PBS group (Figure. S9), showing that the spontaneous fluorescence was very weak and the background fluorescence could be negligible. These results indicated that EF and 6F are suitable for gut microbiota imaging.

Usually, a higher $\varepsilon \times QY$ means better fluorescent performance. Although both EF and 6F could achieve imaging of gut microbiota *in vitro* and *in vivo*, the $\varepsilon \times QY$ of 6F was almost four times higher than that of EF (Table 1). Moreover, the $\varepsilon \times QY$ of 6F in simulated intestinal fluid is also higher than that of EF (Figure. S10). In addition, the synthesis of 6F was only one step, which had an extra lower cost than that of EF. Therefore, 6F is more suitable for gut microbiota imaging.

3. CONCLUSIONS

In conclusion, two positively charged fluorescent dyes, EF and 6F, were synthesized to label bacteria. They could quickly label Gram-positive and Gram-negative bacterial species *in vitro*. Furthermore, the distal ileum and colon microbiota were well labeled after intragastric administration. In addition, both showed no apparent toxicity in *in vitro* and *in vivo* studies. This provides a basis for subsequent studies of monitoring bacterial dynamics *in vivo*. Compared with EF, 6F exhibited excellent fluorescence properties and had a more straightforward synthetic route. This prompted us to optimize the synthetic pathway to develop better quality fluorescent probes. Therefore, 6F was a better dye for future gut microbiota imaging. In summary, our work provided a new microbiota imaging dye, 6F, and a new probe design strategy for fluorescent bacteria imaging.

4. MATERIALS AND METHODS

4.1. Materials and Synthesis. *Reagents.* All of the reagents in this work were purchased from commercial suppliers.

Bacteria. S. aureus (ATCC 25923), E. coli (ATCC 25922), S. pullorum (clinical isolates), and K. peneumoniae (clinical isolates) were preserved in our laboratory. L. reuteri was obtained from the Metabolic Disease Research Center, Chinese Academy of Sciences, Shanghai, 201203, China.

Animals. All animal study procedures were agreed with the Shanghai Experimental Animal Center of Chinese Academy of Sciences guidelines and performed under the institutional guidelines for animal handling. All operations related to animal experiments follow the relevant requirements of the Institutional Animal Care and Use Committee (IACUC) of Shanghai Institute of Material Medica, Chinese Academy of Sciences. BALB/c mice (5−7 weeks old, 18−20 g, ♀) were purchased from Shanghai Experimental Animal Center of Chinese Academy of Sciences. Mice were housed under specific pathogen-free conditions. The feeding environment is 25 °C, 35−45% humidity, and 12 h light-dark alternation. All animals can drink water and eat freely.

Instruments. Biosafety cabinet (Protect-1FD, Thermo-Fisher SCIENTIFIC, USA). Biochemical incubator (SHP-150, Shanghai Jing Hong, Shanghai, China). Preparative high-performance liquid chromatography (HPLC) was performed on a SHIMADZU LC-20AR Instrument with PDA detection.

Scheme 1. Synthesis of EF and 6F[a]
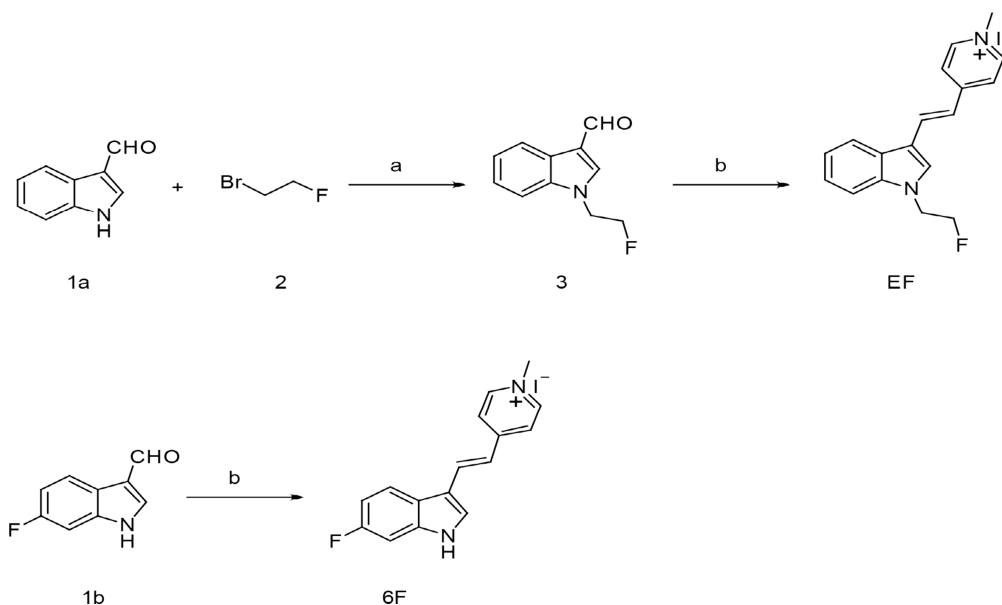
[a]Reagents and conditions: (a) K_2CO_3, KI, DMF, 90 °C; (b) 1, 4-dimethylpyridinium iodide, piperidine, CH_3CN, reflux.

Medical refrigerator (YC-968l, MELNG, Hefei, China). Incubator shaker (YZ-200B, LONGYUE, Shanghai, China). Scanning confocal microscopy (LSM710, Zeiss, Germany). IVIS Lumina system (Perknelmer, Germany).

Synthesis. The general procedure for compounds is presented in Scheme 1. All chemicals and solvents used in the experiment were purchased from commercial suppliers and used without further purification. The reactions were monitored by high-performance liquid chromatography (HPLC) using 254 and 300 nm as the detection wavelength. Flash column chromatography was carried out on a Biotage Isolera Prime purification unit by using commercially prepacked 40−60 μm silica columns. ^{1}H NMR and ^{13}C NMR spectra were recorded on a Bruker 400 NMR spectrometer using chloroform-d (CDCl3) or dimethyl sulfoxide (DMSO-d_6) as a solvent. Chemical shifts were reported in δ (ppm) values, and coupling constants (J) were recorded in hertz (Hz). ESI-MS spectra were collected on a Thermo Scientific TSQ-50002QUANTIVA mass spectrometer. EE and EF were purified on semipreparative HPLC (Waters, XBridge BEH C18, 10 × 250 mm, 5 μm) with CH3CN/water as the mobile phase. The purity was determined by analytical HPLC (Shimadzu, Shim-pack GIST C18, 4.6 × 250 mm, 5 μm) using methanol/buffer (0.1% trifluoroacetic acid in water) as mobile phase.

1-(2-Fluoroethyl)-1H-indole-3-carbaldehyde (3). To a stirred solution of indole-3-aldehyde (1.74 g, 12.0 mmol) in 30 mL of DMF were added 1-fluoro-2-bromoethane (0.9 mL, 12.0 mmol), K_2CO_3 (1.99 g, 14.4 mmol), and KI (0.1 g, 0.6 mmol) were added. The reaction was heated at 90 °C overnight and monitored by HPLC. After the reaction was completed, 150 mL sat. NH_4Cl was added to quench the reaction, and the aqueous mixture was extracted with EtOAc (3 × 75 mL). The combined organic layers were washed twice with brine and concentrated in vacuo. The residue was purified by column chromatography on prepacked silica gel columns to afford pale yellow solid (1.84 g, 80%); ^{1}H NMR (400 MHz, CDCl$_3$) δ 10.03 (s, 1H), 8.38−8.30 (m, 1H), 7.80 (s, 1H),

7.40−7.28 (m, 3H), 4.85 (J = 4.7 Hz, 1H), 4.73 (J = 4.7 Hz, 1H), 4.52 (t, J = 4.7 Hz, 1H), 4.45 (t, J = 4.7 Hz, 1H). ^{13}C NMR (101 MHz, CDCl$_3$) δ: 184.73, 138.79, 137.09, 125.41, 124.28, 123.17, 122.42, 118.81, 109.58, 82.33, 80.61, 47.38, 47.17.

(E)-4-(2-(1-(2-Fluoroethyl)-1H-indol-3-yl)vinyl)-1-methyl-pyridin-1-ium Iodide (EF). A 50 mL oven-dried round-bottom flask was charged with compound 3 (191 mg, 1.0 mmol) and 1, 4-dimethylpyridium iodide (259 mg, 1.1 mmol) in CH_3CN (20 mL). After stirring for 10 min, catalytic amounts of piperidine (0.2 mmol) were added to the mixture. The reaction solution was heated to reflux overnight under an inert atmosphere and monitored by HPLC. After the reaction, the product was purified through recrystallization, and the corresponding precipitate was collected, then washed with cold methanol and recrystallized in acetonitrile, giving orange solid (278 mg, 68%). About 3 mg of the final product was further purified by semipreparative HPLC for the biological test (Waters, XBridge BEH C18, 10 × 250 mm, 5 μm) running a 30 min gradient (H$_2$O/CH$_3$CN = 85/15 for 3 min, then for the next 20 min up to H$_2$O/CH$_3$CN = 5/95 and the last 7 min maintained) with a flow rate of 3 mL/min and with absorbance at λ = 254 and 300 nm. ^{1}H NMR (400 MHz, DMSO-d_6) δ 8.70 (d, J = 6.5 Hz, 2H), 8.24 (d, J = 16.3 Hz, 1H), 8.20 (d, J = 7.6 Hz, 1H), 8.15 (d, J = 6.6 Hz, 2H), 8.01 (s, 1H), 7.67 (d, J = 7.9 Hz, 1H), 7.39−7.25 (m, 3H), 4.85 (t, J = 4.6 Hz, 1H), 4.73 (t, J = 4.6 Hz, 1H), 4.67 (t, J = 4.7 Hz, 1H), 4.60 (t, J = 4.6 Hz, 1H), 4.18 (s, 3H). ^{13}C NMR (101 MHz, DMSO-d_6) δ: 154.00, 144.25, 137.42, 135.36, 134.77, 125.49, 125.45, 123.07, 121.77, 121.47, 120.58, 117.34, 113.06, 111.18, 83.14, 81.81, 46.52, 46.36, 46.30. ESI-MS m/z: [M - I]$^+$ calculated for $C_{18}H_{18}FN_2$: 281.1, found: 281.1.

(E)-4-(2-(6-Fluoro-1H-indol-3-yl)vinyl)-1-methylpyridin-1-ium Iodide (6F). The synthesis of 6F was similar to that of EF. Brown solid (237 mg, 62%). ^{1}H NMR (400 MHz, DMSO-d_6) δ 11.95 (s, 1H), 8.71 (d, J = 6.6 Hz, 2H), 8.22 (d, J = 16.3 Hz, 1H), 8.17 (dd, J = 8.8, 5.3 Hz, 1H), 8.13 (d, J = 6.8 Hz, 2H), 7.98 (s, 1H), 7.38−7.25 (m, 2H), 7.11 (td, J = 9.2, 2.4 Hz,

1H), 4.19 (s, 3H). ^{13}C NMR (101 MHz, DMSO-d_6) δ: 160.29, 158.41, 154.03, 144.27, 137.64, 137.54, 135.59, 132.58, 121.77, 121.65, 121.53, 121.45, 117.28, 113.52, 109.38, 109.19, 98.86, 98.66, 46.31. ESI-MS m/z: [M - I]$^+$ calculated for $C_{16}H_{14}FN_2$: 253.1, found: 253.1.

4.2. Characterization of EF and 6F. Ultraviolet–visible absorbance and fluorescence spectra of EF and 6F were recorded in water.

The molar absorption coefficient (ε) was determined by measuring the absorption value of six different concentrations of EF and 6F, which dissolved in water, and then making a linear fit between the concentration and the absorption value.

For the quantum yield calculation, EF and 6F were dissolved in acetonitrile in 5 different concentrations for absorption and emission spectrum measurement. The fluorescent emission spectra were integrated and plotted against the OD426 values. Then, a linear fit was applied to verify the linearity between the fluorescent intensities and concentrations. DCM (QY$_0$ = 43.5%) in methanol was used as the standard. The quantum yield was determined based on the following equation:

$$QY_S = QY_0 \times \frac{slope_s}{slope_0} \times \left(\frac{n_s}{n_0} \right)^2$$

QY$_S$ is the quantum yield of EF and 6F; QY$_0$ is the QY of DCM; n_0 is the refractive index of the DCM solution, which is methanol (1.33); n_S is the refractive index of EF and 6F solutions, which is acetonitrile (1.34).

The fluorescent stability test used a 30 mW LED light source with a 420–470 nm bandpass filter as the light source. EF and 6F were dissolved in water at a concentration of 20 μM and continuously excited for 60 min. For the first 15 min, the fluorescence intensity was measured every 1 min. For the next 45 min, fluorescence was measured every 5 min. The stability was calculated by measuring fluorescence intensity/starting fluorescence signal ×100%.

4.3. Bacteria Culture. *E. coli*, *S. pullorum*, and *K. pneumoniae* were cultured for 12 h in Luria–Bertani (LB) medium at 37 °C in an incubator shaker (180 rpm/h). *S. aureus* was cultured in a Brain Heart Infusion (BHI) medium. *L. reuteri* was cultured in a Man Rogosa Sharpe (MRS) medium. Then, one single colony was inoculated into 5 mL of fresh medium and cultured to an optical density of 0.6 at 600 nm in the incubator shaker (180 rpm/h).

4.4. Bacterial Viability. A 50 μL portion of the bacteria stains at a concentration of 10^8 was mixed with 0, 2.5, 5, 7.5, 12.5 μL of EF and 6F (200 μM), respectively, into 5 mL of fresh medium and cultured at 37 °C in an incubator shaker (180 rpm/h) for 6 h. Then, the mixture was centrifuged at 6000 rpm for 8 min. The sediment was collected thrice after being washed with a phosphate-balanced solution (PBS) and resuspended in 2 mL PBS. Finally, the suspensions were diluted into different concentrations and inoculated in culture media to calculate colony-forming units (CFUs).

4.5. Confocal Microscopy Imaging. One mL of each bacteria strain at a concentration of 10^6 was mixed with 0.2 mL of EF and 6F (200 μM) respectively into 2 mL of PBS and cultured at 37 °C in an incubator shaker (180 rpm/h) for 30 min. Then the commercial mitochondrial dye Mito-Tracker red (1 μM) and FITC (2.5 μM) were added for 20 min incubation. After 20 min, the medium was removed, and bacteria were washed with 1 mL of PBS 5 times. Finally, 10 μL of the resuspended bacteria were added to the glass slide. The glass slide was performed on a confocal laser microscope. The whole process was protected from light.

4.6. Animal Handling. Mice were randomly selected from cages for all experiments. No blinding was performed. All groups within the study contained $n \geq 3$ mice.

4.7. Statistical Analysis. All data were expressed as mean ± SD (standard deviation). The fluorescent images were analyzed using ImageJ 1.8.0 (NIH, Bethesda, MD). ROI analysis was performed by drawing a shape around the specific site and using the software to calculate the mean pixel intensity. Statistical analysis was performed with SPSS software, version 23.0 (SPSS Inc.). A two-tailed test $P < 0.05$ was considered to be statistically significant.

■ ASSOCIATED CONTENT

Ⓢ Supporting Information

The Supporting Information is available free of charge at https://pubs.acs.org/doi/10.1021/acsomega.4c03727.

> Supporting figures for experimental results, HPLC spectra of EF and 6F, and the NMR and mass spectra (PDF)

■ AUTHOR INFORMATION

Corresponding Authors

Xin Feng − *State Key Laboratory for Diagnosis and Treatment of Severe Zoonotic Infectious Diseases, and College of Veterinary Medicine, Jilin University, Changchun 130062, China*; Email: feng_xin@jlu.edu.cn

Hao Chen − *State Key Laboratory of Chemical Biology, Molecular Imaging Center, Shanghai Institute of Materia Medica, Chinese Academy of Sciences, Shanghai 201203, China*; ⓞ orcid.org/0000-0002-8470-5467; Email: haoc@simm.ac.cn

Authors

Yue Liu − *State Key Laboratory for Diagnosis and Treatment of Severe Zoonotic Infectious Diseases, and College of Veterinary Medicine, Jilin University, Changchun 130062, China*; ⓞ orcid.org/0009-0003-5772-4122

Zhiming Wang − *State Key Laboratory of Chemical Biology, Molecular Imaging Center, Shanghai Institute of Materia Medica, Chinese Academy of Sciences, Shanghai 201203, China*

Ke Li − *State Key Laboratory for Diagnosis and Treatment of Severe Zoonotic Infectious Diseases, and College of Veterinary Medicine, Jilin University, Changchun 130062, China*

Ruihu Song − *State Key Laboratory of Chemical Biology, Molecular Imaging Center, Shanghai Institute of Materia Medica, Chinese Academy of Sciences, Shanghai 201203, China*

Zhiqiang Xu − *State Key Laboratory for Diagnosis and Treatment of Severe Zoonotic Infectious Diseases, and College of Veterinary Medicine, Jilin University, Changchun 130062, China*

Tianhe Yu − *State Key Laboratory for Diagnosis and Treatment of Severe Zoonotic Infectious Diseases, and College of Veterinary Medicine, Jilin University, Changchun 130062, China*

Jing Wang − *Radiology Department, the First Hospital of Jilin University, Changchun 130021, China*

Complete contact information is available at:
https://pubs.acs.org/10.1021/acsomega.4c03727

Author Contributions

¶Y.L. and Z.W. contributed equally to this work

Notes

The authors declare no competing financial interest.

■ REFERENCES

(1) Clemente, J. C.; Ursell, L. K.; Parfrey, L. W.; Knight, R. The impact of the gut microbiota on human health: an integrative view. *Cell* **2012**, *148*, 1258.

(2) Fan, Y.; Pedersen, O. Gut microbiota in human metabolic health and disease. *Nat. Rev. Microbiol.* **2021**, *19*, 55.

(3) Sherwin, E.; Bordenstein, S. R.; Quinn, J. L.; Dinan, T. G.; Cryan, J. F. Microbiota and the social brain. *Science* **2019**, *366*, eaar2016.

(4) Pedersen, H. K.; Forslund, S. K.; Gudmundsdottir, V.; Petersen, A. O.; Hildebrand, F.; Hyotylainen, T.; Nielsen, T.; Hansen, T.; Bork, P.; Ehrlich, S. D.; Brunak, S.; Oresic, M.; Pedersen, O.; Nielsen, H. B. A computational framework to integrate high-throughput 'omics' datasets for the identification of potential mechanistic links. *Nat. Protoc* **2018**, *13*, 2781.

(5) Qin, J.; Li, R.; Raes, J.; Arumugam, M.; Burgdorf, K. S.; Manichanh, C.; Nielsen, T.; Pons, N.; Levenez, F.; Yamada, T.; Mende, D. R.; Li, J.; Xu, J.; Li, S.; Li, D.; Cao, J.; Wang, B.; Liang, H.; Zheng, H.; Xie, Y.; Tap, J.; Lepage, P.; Bertalan, M.; Batto, J. M.; Hansen, T.; Le Paslier, D.; Linneberg, A.; Nielsen, H. B.; Pelletier, E.; Renault, P.; Sicheritz-Ponten, T.; Turner, K.; Zhu, H.; Yu, C.; Li, S.; Jian, M.; Zhou, Y.; Li, Y.; Zhang, X.; Li, S.; Qin, N.; Yang, H.; Wang, J.; Brunak, S.; Dore, J.; Guarner, F.; Kristiansen, K.; Pedersen, O.; Parkhill, J.; Weissenbach, J.; Meta, H. I. T. C.; Bork, P.; Ehrlich, S. D.; Wang, J. A human gut microbial gene catalogue established by metagenomic sequencing. *Nature* **2010**, *464*, 59.

(6) Donaldson, G. P.; Lee, S. M.; Mazmanian, S. K. Gut biogeography of the bacterial microbiota. *Nat. Rev. Microbiol* **2016**, *14*, 20.

(7) Tropini, C.; Earle, K. A.; Huang, K. C.; Sonnenburg, J. L. The Gut Microbiome: Connecting Spatial Organization to Function. *Cell Host Microbe* **2017**, *21*, 433.

(8) McCallum, G.; Tropini, C. The gut microbiota and its biogeography. *Nat. Rev. Microbiol.* **2024**, *22*, 105.

(9) Lin, L.; Du, Y.; Song, J.; Wang, W.; Yang, C. Imaging Commensal Microbiota and Pathogenic Bacteria in the Gut. *Acc. Chem. Res.* **2021**, *54*, 2076.

(10) Lim, B.; Zimmermann, M.; Barry, N. A.; Goodman, A. L. Engineered Regulatory Systems Modulate Gene Expression of Human Commensals in the Gut. *Cell* **2017**, *169*, 547.

(11) Whitaker, W. R.; Shepherd, E. S.; Sonnenburg, J. L. Tunable Expression Tools Enable Single-Cell Strain Distinction in the Gut Microbiome. *Cell* **2017**, *169*, 538.

(12) Barbier, M.; Bevere, J.; Damron, F. H. In Vivo Bacterial Imaging Using Bioluminescence. *Methods Mol. Biol.* **2018**, *1790*, 87.

(13) Johansson, M. E.; Hansson, G. C. Preservation of mucus in histological sections, immunostaining of mucins in fixed tissue, and localization of bacteria with FISH. *Methods Mol. Biol.* **2012**, *842*, 229.

(14) Imai, Y.; Meyer, K. J.; Iinishi, A.; Favre-Godal, Q.; Green, R.; Manuse, S.; Caboni, M.; Mori, M.; Niles, S.; Ghiglieri, M.; Honrao, C.; Ma, X.; Guo, J. J.; Makriyannis, A.; Linares-Otoya, L.; Bohringer, N.; Wuisan, Z. G.; Kaur, H.; Wu, R.; Mateus, A.; Typas, A.; Savitski, M. M.; Espinoza, J. L.; O'Rourke, A.; Nelson, K. E.; Hiller, S.; Noinaj, N.; Schaberle, T. F.; D'Onofrio, A.; Lewis, K. A new antibiotic selectively kills Gram-negative pathogens. *Nature* **2019**, *576*, 459.

(15) Wang, W.; Chen, X. Antibiotics-based fluorescent probes for selective labeling of Gram-negative and Gram-positive bacteria in living microbiotas. *Science China Chemistry* **2018**, *61*, 792.

(16) Wang, W.; Zhu, Y.; Chen, X. Selective Imaging of Gram-Negative and Gram-Positive Microbiotas in the Mouse Gut. *Biochemistry* **2017**, *56*, 3889.

(17) Faber, F.; Tran, L.; Byndloss, M. X.; Lopez, C. A.; Velazquez, E. M.; Kerrinnes, T.; Nuccio, S. P.; Wangdi, T.; Fiehn, O.; Tsolis, R. M.; Baumler, A. J. Host-mediated sugar oxidation promotes post-antibiotic pathogen expansion. *Nature* **2016**, *534*, 697.

(18) Rivera-Chavez, F.; Zhang, L. F.; Faber, F.; Lopez, C. A.; Byndloss, M. X.; Olsan, E. E.; Xu, G.; Velazquez, E. M.; Lebrilla, C. B.; Winter, S. E.; Baumler, A. J. Depletion of Butyrate-Producing Clostridia from the Gut Microbiota Drives an Aerobic Luminal Expansion of Salmonella. *Cell Host Microbe* **2016**, *19*, 443.

(19) Wang, W.; Lin, L.; Du, Y.; Song, Y.; Peng, X.; Chen, X.; Yang, C. J. Assessing the viability of transplanted gut microbiota by sequential tagging with D-amino acid-based metabolic probes. *Nat. Commun.* **2019**, *10*, 1317.

(20) Pasquina-Lemonche, L.; Burns, J.; Turner, R. D.; Kumar, S.; Tank, R.; Mullin, N.; Wilson, J. S.; Chakrabarti, B.; Bullough, P. A.; Foster, S. J.; Hobbs, J. K. The architecture of the Gram-positive bacterial cell wall. *Nature* **2020**, *582*, 294.

(21) Hu, F.; Qi, G.; Kenry; Mao, D.; Zhou, S.; Wu, M.; Wu, W.; Liu, B. Visualization and In Situ Ablation of Intracellular Bacterial Pathogens through Metabolic Labeling. *Angew. Chem., Int. Ed. Engl.* **2020**, *59*, 9288.

(22) Nekhotiaeva, N.; Elmquist, A.; Rajarao, G. K.; Hallbrink, M.; Langel, U.; Good, L. Cell entry and antimicrobial properties of eukaryotic cell-penetrating peptides. *FASEB J.* **2004**, *18*, 394.

(23) Bullok, K. E.; Gammon, S. T.; Violini, S.; Prantner, A. M.; Villalobos, V. M.; Sharma, V.; Piwnica-Worms, D. Permeation peptide conjugates for in vivo molecular imaging applications. *Mol. Imaging* **2006**, *5*, 1.

(24) Maslov, I.; Bogorodskiy, A.; Mishin, A.; Okhrimenko, I.; Gushchin, I.; Kalenov, S.; Dencher, N. A.; Fahlke, C.; Buldt, G.; Gordeliy, V.; Gensch, T.; Borshchevskiy, V. Efficient non-cytotoxic fluorescent staining of halophiles. *Sci. Rep* **2018**, *8*, 2549.

(25) Zhang, C.; Meng, J.; Zhang, Y.; Huang, D.; Yan, P.; Tan, B.; Jiang, H.; Deng, Z. FITC characterization of a cathepsin B-responsive nanoprobe for report of differentiation of HL60 cells into macrophages. *J. Pept Sci.* **2022**, *28*, No. e3371.

(26) Apostolos, A. J.; Chordia, M. D.; Kolli, S. H.; Dalesandro, B. E.; Rutkowski, M. R.; Pires, M. M. Real-time non-invasive fluorescence imaging of gut commensal bacteria to detect dynamic changes in the microbiome of live mice. *Cell Chem. Biol.* **2022**, S2451.

(27) Chen, H.; Wang, J.; Feng, X.; et al. Mitochondria-targeting fluorescent moleculesfor high efficiency cancer growth inhibition and imaging[J]. *Chem. Sci.* **2019**, *10*, 7946.

(28) Chen, H.; Wang, J.; Feng, X.; Zhu, M.; Hoffmann, S.; Hsu, A.; Qian, K.; Huang, D.; Zhao, F.; Liu, W.; Zhang, H.; Cheng, Z. Mitochondria-targeting fluorescent molecules for high efficiency cancer growth inhibition and imaging. *Chem. Sci.* **2019**, *10*, 7946.

(29) Zheng, L.; Wang, Z.; Zhang, X.; Zhou, Y.; Ji, A.; Lou, H.; Liu, X.; Chen, H.; Cheng, Z. Development of Mitochondria-Targeted Small-Molecule Dyes for Myocardial PET and Fluorescence Bimodal Imaging. *J. Med. Chem.* **2022**, *65*, 497.

(30) Joseph, L.; Merciecca, T.; Forestier, C.; Balestrino, D.; Miquel, S. From Klebsiella pneumoniae Colonization to Dissemination: An Overview of Studies Implementing Murine Models. *Microorganisms* **2021**, *9*, 1282.

(31) Takao, M.; Kawaguchi, Y.; Matsumura, M.; Kazami, Y.; Tanimoto, M.; Abe, S.; Maki, H.; Ishizawa, T.; Arita, J.; Akamatsu, N.; Kaneko, J.; Kokudo, N.; Hasegawa, K. Probe-based confocal laser endomicroscopy for real-time evaluation of colorectal liver metastasis in resected surgical specimens. *Hum Cell.* **2023**, *36*, 2066.